Article ID: 1006-8775(2021) 01-0070-11

Characteristics of Atmospheric Heat Sources in the Tibetan Plateau–Tropical Indian Ocean Region

LUO Xiao-qing (罗小青)[1, 2], XU Jian-jun (徐建军)[1, 2], LIU Chun-lei (刘春雷)[1, 2], ZHANG Yu (张 宇)[1,2], LI Kai (李 凯)[3], WU Lang-qi (巫朗琪)[2]

(1. South China Sea Institute of Marine Meteorology, Guangdong Ocean University, Zhanjiang, Guangdong 524088 China; 2. College of Ocean and Meteorology, Guangdong Ocean University, Zhanjiang, Guangdong 524088 China; 3. Maritime College, Guangdong Ocean University, Zhanjiang, Guangdong 524088 China)

Abstract: Investigating the temporal and spatial distributions of the atmospheric heat sources (AHS) over the Tibetan Plateau-Tropical Indian Ocean (TP-TIO) region is of great importance for the understanding of the evolution and development of the South Asian summer monsoon (SASM). This study used the Japanese 55-year Reanalysis (JRA-55) data from 1979 to 2016 and adopted statistical methods to study the characteristics of the AHS between the TP and TIO, and theirs link to the SASM on an interannual scale. The results indicated that the monthly variations of the AHS in the two regions were basically anti-phase, and that the summer AHS in the TP was obviously stronger than that in the TIO. There were strong AHS and atmospheric moisture sink (AMS) centers in both the eastern and western TP in summer. The AHS center in the east was stronger than that in the west, and the AMS centers showed the opposite pattern. In the TIO, a strong AHS center in the northwest-southeast direction was located near 10°S, 90°E. Trend analysis showed that summer AHS in the TIO was increasing significantly, especially before 1998, whereas there was a weakening trend in the TP. The difference of the summer AHS between the TP and TIO (hereafter IQ) was used to measure the thermal contrast between the TP and the TIO. The IQ showed an obvious decreasing trend. After 1998, there was a weak thermal contrast between the TP and the TIO, which mainly resulted from the enhanced AHS in the TIO. The land-sea thermal contrast, the TIO Hadley circulation in the southern hemisphere and the SASM circulation all weakened, resulting in abnormal circulation and abnormal precipitation in the Bay of Bengal (BOB).

Key words: atmospheric heat sources; Tibetan Plateau; Tropical Indian Ocean; land-sea thermal contrast

CLC number: P465 **Document code:** A

https://doi.org/10.46267/j.1006-8775.2021.007

1 INTRODUCTION

The atmospheric heat sources (AHS), also known as the apparent heat sources, are the sum of the surface sensible heat, precipitation condensation latent heat, and net atmospheric radiation (Yanai et al. [1]). The AHS are the heat engines driving the planetary scale circulation (Yanai and Tomita [2]). There is strong AHS in the Asian monsoon region in summer (Li and Yanai [3]), and the spatial distribution of AHS determines the atmospheric circulation (Wu and Liu [4]) which affects the weather systems and precipitation (Yao et al. [5]).

Submitted 2020-10-10; **Revised** 2020-11-15; **Accepted** 2021-02-15

Funding: Strategic Priority Research Program of Chinese Academy of Sciences (XDA20060501); 2019 Non-funded Science and Technology Research Project of Zhanjiang (20051817454-6338); 2020 Guangdong Ocean University College Student Innovation and Entrepreneurship Project (580520153)

Biography: LUO Xiao-qing, Ph. D. candidate, primarily undertaking research on sea-land-air interaction.

Corresponding author: XU Jian-jun, e-mail: jxu@gdou.edu.cn

The thermal condition of the Tibetan Plateau (TP) and the tropical Indian Ocean (TIO) are the two key interactive systems that modulate Asian monsoon. As the 'Third Pole' of the world, the TP has an average elevation of more than 4 km and spans about 31 longitudes. The formation and maintenance of the South Asian High (Ye and Zhang [6]) and the onset of the South Asian summer monsoon (SASM) are closely related to the thermodynamic effects of the TP (Wu and Zhang [7]). Studies on the TP AHS, including quantitative estimation of the AHS (Luo and Xu [8]; Luo et al. [9]; Xie et al. [10]), and determination of its vertical structure (Yanai and Tomita [2]; Zhong et al. [11]), spatial and temporal distributions (Jiang et al. [12]; Yanai et al. [1]; Zhao and Cheng [13]) have got many conclusions. Hu and Duan have suggested that the influence of the AHS in the TP on the East Asian summer monsoon precipitation is more important than the tropical Indian Ocean Basin mode [14]. The thermal condition of the TIO also has an impact on the interannual variability of the East Asian summer monsoon (Huang et al. [15]) and the TP AHS (Jiang et al. [12]; Ji et al. [16]). Meanwhile, the interannual variation of summer AHS over the central and eastern TP is significantly affected by convection around the

western Maritime Continent (Jiang et al. [12]). Model results indicate that the TP heating regulates the Asian monsoon circulation through air-sea interactions (He et al. [17]; Wang et al. [18]).

The thermodynamic equations show that the local temperature changes are the result of horizontal advection, vertical transportation, and AHS. In most previous studies, the atmospheric temperature was chosen as the index to study the land-sea thermal contrast (Dai et al. [19]), yet the distribution of temperature is inconsistent with the heat sources. Hence, the thermal contrast between the TP and the TIO is an important factor for studying the SASM. The greater the land-sea thermal contrast, the stronger the SASM circulation.

Despite these works, our understanding of the thermal effect of the TP-TIO region on the SASM remains insufficient, since the AHS in this region has been discussed widely but often separately. The seasonal variability of the TP AHS is out of phase with the TIO AHS (Zhang et al. [20]), and the summer AHS shows significant meridional gradient in this region (Zhang et al. [21]). The purpose of the present study is to investigate temporal and spatial distributions of the AHS in the TP and the TIO, and theirs link to the SASM on an interannual scale. In the rest of this paper, the data and methods are described in sections 2 and 3, respectively. Section 4 gives the results, and the summary and discussion are provided in section 5.

2 DATA

The data used in this study are as follows.

(1) Station data. We used data from 133 observation stations (Fig. 1) provided by the China Meteorology Administration (CMA). Variables include 2-m air temperature, surface temperature, 10-m wind speed, and precipitation from 1980 to 2012. All these data went through quality-control procedures to eliminate erroneous data and ensure homogeneity. Then the station data were interpolated to the grid points to calculate the AHS.

(2) Satellite radiation data from the Global Energy and Water Exchanges-Surface Radiation Budget (GEWEX-SRB) with a resolution of 1.0° × 1.0° . Radiation fluxes included the downward and upward shortwave and longwave fluxes at both the top of the atmosphere and the surface. The monthly net atmospheric radiation was calculated from 1984 to 2008. According to the direct method (see section 3), we can use station data and satellite data to obtain the AHS on the TP (75°E−103°E, 28°N−38°N) from 1984 to 2008.

(3) Four sets of monthly reanalysis data: the ERA-Interim (ERA-I) data from the European Centre for Medium-Range Weather Forecasts with a resolution of 0.75° × 0.75° (Dee et al. [22]), the Japanese 55-year Reanalysis (JRA-55) data from the Japan Meteorological Agency (JMA) with a resolution of 1.25° × 1.25° (Kobayashi et al. [23]), the MERRA2 data from the NASA Goddard Space Flight Center with a resolution of 0.67° × 0.5° (Gelaro et al. [24]), and the National Centers for Environmental Prediction / Department of Energy (NCEP / DOE) data with a resolution of 2.5° × 2.5° (Kanamitsu et al. [25]). The present study calculated AHS and atmospheric moisture sources (AMS) by using horizontal wind, vertical wind, temperature, specific humidity on pressure levels and the surface pressure in the domain 30°E−120°E, 20°S−45°N from 1980 to 2016 with four reanalysis datasets.

(4) Global Precipitation Climatology Project (GPCP) precipitation data. This is a monthly precipitation dataset from 1979 to the present that combines data from rain gauge stations, satellites, and sounding observations into 2.5° × 2.5° global grids.

(5) The monthly outgoing longwave radiation data from the National Oceanic and Atmospheric Administration with a resolution of 2.5° × 2.5°, and the geopotential height data from NCEP / DOE with a resolution of 2.5° × 2.5°.

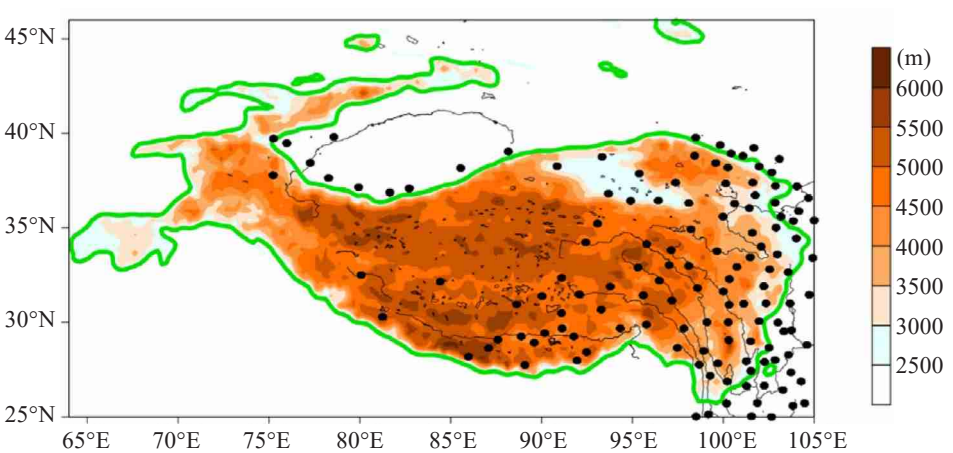

Figure 1. The 133 observation stations. The black spots represent stations, the black curve lines and green curve lines represent rivers and altitude≥2500m, respectively, and the shading indicates the topography (m).

3 METHODOLOGY

3.1 *Method to determine the AHS and AMS* (Luo and Xu [8])

The AHS is the sum of surface sensible heating, condensation heating, and radiative heating based on direct method (formula (1)), and $<Q_1>$ is the vertically integrated AHS. Similarly, the AMS is defined by formula (5) and $<Q_2>$ is the vertically integrated AMS. The components of $<Q_1>$ are obtained from formulas (2)-(4), respectively. Q_L, Q_{SH}, and $<Q_R>$ are condensation heating, surface sensible heating, and vertically integrated radiative heating, respectively.

$$<Q_1>=<Q_R>+Q_{\mathrm{SH}}+Q_L \tag{1}$$

$$<Q_R>=(S_\infty^{\downarrow}-S_\infty^{\uparrow})-(S_0^{\downarrow}-S_0^{\uparrow})-(F_0^{\downarrow}-F_0^{\uparrow})-F_\infty \tag{2}$$

$$Q_{\mathrm{SH}}=c_p\rho_{\mathrm{air}}C_{\mathrm{D}}V_{10}(T_{\mathrm{s}}-T_{\mathrm{a}}) \tag{3}$$

$$Q_L=P_r\times L\times\rho_w \tag{4}$$

$$<Q_2>=L(P_r-E) \tag{5}$$

In the above formula, angle brackets represent the integration of the whole atmosphere. S and F are the shortwave and longwave radiative fluxes. The subscripts "∞" and "0" represent the fluxes at the top of the atmosphere and at the surface of the Earth. Upward arrows denote upward radiative fluxes, and vice versa. c_p =1004J kg^{-1} K^{-1} and it is the drag coefficient for heat, and C_D=0.004 and it is the specific heat of dry air at constant pressure. ρ_{air} and ρ_w are air density and water density, respectively. T_{s}, T_{a}, V_{10}, P_r and E represent the surface temperature, 2-m air temperature, 10-m wind speed, precipitation, and evaporation, respectively. L= 2.5 × 10^{6}J kg^{-1} and it is the condensation heating coefficient.

The indirect method is also called the "residual diagnosis method". $<Q_1>$ and $<Q_2>$ are defined by formulas (6) and (7), which are the sum of the local variation term, the advection variation term, and the vertical variation term. According to formulas (6) and (7), we can obtain the AHS and AMS at each layer, also known as the heating rate (K d^{-1}). The overbar in the formulae represents the regional average value. θ and q are potential temperature (K) and specific humidity (g kg^{-1}), respectively. $\vec{V}$ and ω are horizontal wind speed (m·s^{-1}) and vertical velocity (Pa s^{-1}).

$$<Q_1>=\frac{c_{\mathrm{p}}}{g}\int_{p_T}^{p_{\mathrm{s}}}\left[\left(\frac{p}{p_0}\right)^k\left(\frac{\partial\bar{\theta}}{\partial t}+\vec{V}\cdot\nabla\bar{\theta}+\bar{\omega}\frac{\partial\bar{\theta}}{\partial p}\right)\right]\mathrm{d}p \tag{6}$$

$$<Q_2>=-L\frac{c_{\mathrm{p}}}{g}\int_{p_T}^{p_{\mathrm{s}}}\left[\left(\frac{\partial\bar{q}}{\partial t}+\vec{V}\cdot\nabla\bar{q}+\bar{\omega}\frac{\partial\bar{q}}{\partial p}\right)\right]\mathrm{d}p \tag{7}$$

For simplicity, we used Q_1 to represent $<Q_1>$ and Q_2 to represent $<Q_2>$ hereafter. A value of Q_1 greater (less) than zero indicates that the atmosphere has a net heat gain (loss). In general, a positive value of Q_1 is called a heat source and a negative value is called a heat sink. A value of Q_2 greater (less) than zero means that there is a net moisture loss (gain). If the spatial distributions of Q_1 and Q_2 are consistent and both are positive, this indicates that the AHS is mainly dominated by precipitation latent heating. Section 4 shows the AHS as Q_1 and the AMS as Q_2 for simplicity. According to formula (1), the present study used station data, radiation data and four reanalysis data to calculate the AHS of the TP in the 75° E−103° E, 28° N−38° N area. Meanwhile, reanalysis data based on formula (6) and formula (7) were used to calculate the AHS and AMS in the 20° S−45°N, 30°E−120°E area. The TIO is defined in the 15°S−5°N, 60°E−100°E area.

3.2 *Screening data*

The Pearson correlation coefficient (r_{kl}) defined by formula (8) is used to measure the correlation between the observed AHS values and those from the four reanalysis data. In formula (8), x is the AHS, and r_{kl} is the correlation coefficient calculated from observational data (k) and reanalysis data (l), respectively. Temporal correlation coefficients in Fig. 2 and Table 1 were calculated after averaging the AHS over the TP (75°E−103°E, 28°N−38°N) which maskouts the altitude ≥2500m for observational and reanalysis data from 1984−2008.

$$r_{\mathrm{kl}}=\frac{\sum_{i=1}^{n}(x_{\mathrm{ki}}-\bar{x}_k)(x_{\mathrm{li}}-\bar{x}_l)}{\sqrt{\sum_{i=1}^{n}(x_{\mathrm{ki}}-\bar{x}_k)^2}\sqrt{\sum_{i=1}^{n}(x_{\mathrm{li}}-\bar{x}_l)^2}} \tag{8}$$

Figure 2 shows that the correlation coefficient is greater in July-September while the JRA-55 dataset is the greatest among the four reanalysis datasets. In summer, the correlation coefficients all have passed the 95% significance test except for the MERRA2 with indirect method (Table 1). The JRA-55 dataset not only assimilates the upper tropospheric atmospheric observations but also uses a 4D assimilation technique for the upper tropospheric observations since 1958 (Fujiwara et al. [26]). Hence, we can see that no matter which method is used, the JRA-55 data shows the best correlation with the observational data (Table 1). Hu and Duanalso concluded that the JRA-55 data can best describe the TP thermal heating [14].

On the basis of the above analysis, and in view of the scarcity of observational data in the TP, we used the JRA-55 data to further study the temporal and spatial characteristics of the AHS in the TP-TIO region, and theirs link to the SASM.

3.3 *Selecting the study area*

The TP (75°E−103°E, 28°N−38°N) and TIO (15°S−5° N, 60° E−100° E) regions are located to the south and the north of the SASM respectively. The Asian monsoon regions are heat sources in summer, while the TP and TIO are strong heat source centers along their latitudes (Fig. 3). The TP has a strong heat source center, with the maximum heating (Q_1≥300 W m^{-2}) located on the southern slope of the TP, and the TIO maximum also

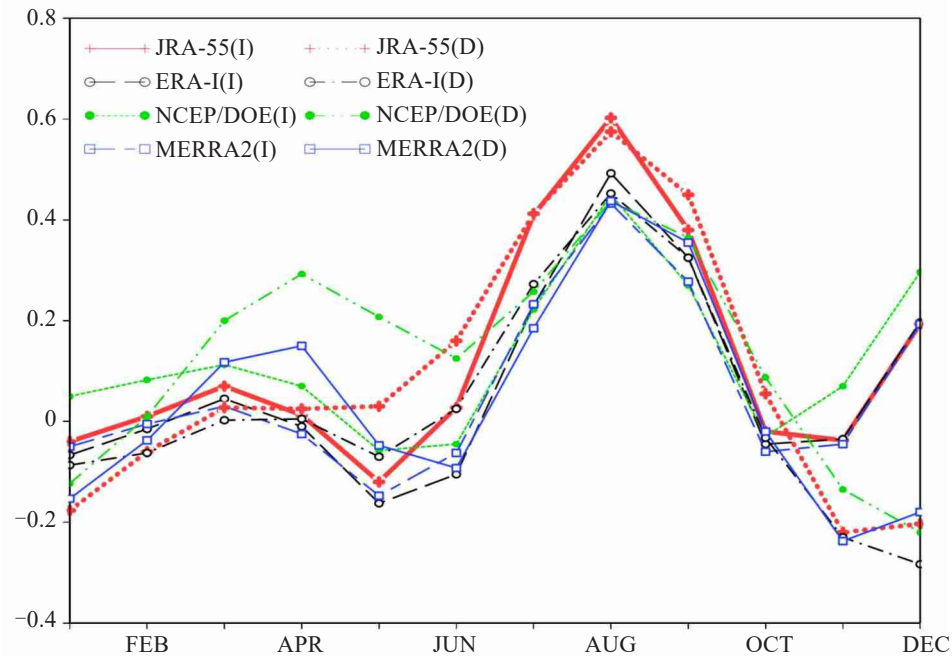

Figure 2. The monthly variations of correlation coefficients for Q_1 between the observational data and those from four reanalysis datasets from 1984 to 2008 on the TP (The average area is in the 75°E−103°E, 28°N−38°N which maskouts the altitude ≥2500m; I and D represent the indirect method and the direct method, respectively).

Table 1. The correlation coefficients for the summer Q_1 on the TP (The average area is in the 75° E−103° E, 28° N−38° N which maskouts the altitude ≥2500m) between the observations and the four reanalysis datasets based on two methods (Italics indicate a correlation coefficient does not pass the 95% significance test).

		JRA-55	NCEP/DOE	ERA-I	MERRA2
Observed data	Direct method	0.611	0.546	0.483	0.490
	Indirect method	0.634	0.585	0.492	*0.312*

reaches 300 W m^{-2} in the south of the equator. The AHS in the TP is accompanied by lower wind convergence, while the AHS in the TIO is located in the area of southeast trade winds and equatorial westerly winds (Fig. 3(a) and (b)). Studies have shown that the TP thermal forcing and the zonal land-sea thermal contrast between East Asia and the Pacific region have a profound influence on the East Asian monsoon system (He et al. [27]; Zhang et al. [28]); therefore, it is necessary to study the meridional thermal contrast between the TP and the TIO.

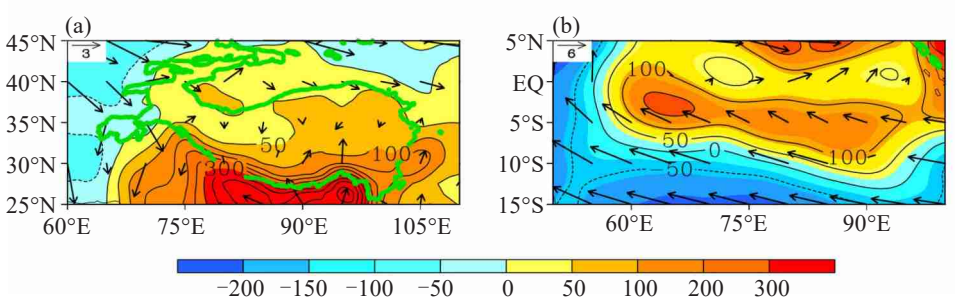

Figure 3. The zonal anomaly Q_1 (shaded, W m^{-2}) and horizontal wind (vector, m s^{-1}) in summer during 1980−2016. (a) The TP and winds at 650 hPa, and (b) the TIO and winds at 850 hPa. The green curve represents altitude ≥2500 m.

4 RESULTS

4.1 *Seasonal variation of heat sources*

The seasonal variations of AHS in the TP and the TIO are almost reversed (Fig. 4). The TP is a heat source from April to September and that the strongest intensity is in July (Q_1 = 113 W m^{-2}), while the TIO AHS gets the minimum in June (Q_1=46W m^{-2}) and the maximum in January (Q_1 = 163 W m^{-2}). In summer, the TP AHS is mainly dominated by precipitation latent heat, which

coincides with the strongest precipitation in July (Feng and Zhou [29]). Therefore, the TP AHS reaches the maximum in July. The TP is a cold source in winter and the strongest intensity is in January (Q_1 = −113 W m^{-2}), which is consistent with the monthly AHS variation in Duan et al. [30]. However, quantitative estimations of the monthly AHS in previous studies (Yanai et al. [1]; Zhao and Chen [13]; Ji et al. [16]) are considerably different, which may be due to differences in regions, calculation methods, data, study periods, and so on (Liu and Li [31]). For the TIO, it's a heat source all year round due to the convection precipitation latent heat. The standard errors of AHS in the TP and TIO are 78.97 and 38.56 respectively, which indicate that the seasonal variability in the TP is more obvious.

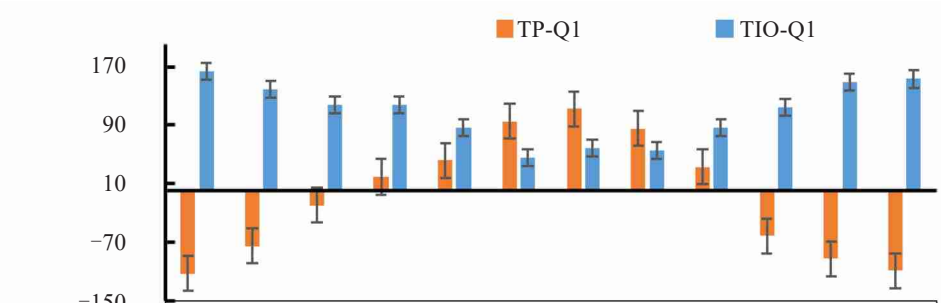

	1	2	3	4	5	6	7	8	9	10	11	12
TP-Q1	−113	−76	−20	19	42	95	113	85	33	−62	−92	−109
TIO-Q1	163	139	117	118	87	46	58	55	86	115	148	153

Figure 4. The monthly variations of Q_1 from 1980 to 2016 in the TP (The area is in the 75°E−103°E, 28°N−38°N which maskouts the altitude ≥2500m) and the TIO (60°E−100°E, 15°S−5°N) (Black bars indicate the standard error; units: W m^{-2}).

In Fig. 5(a1), the heat sources center in the east and west of the TP from March to September and are strongest in summer. The intensity is stronger, and the extent is wider for the eastern heat sources center than those for the western heat source center, and $Q_1 \geq 100$ W m^{-2} occurs in the east from May to July but only occurs in July in the west. The AMS intensity in the western part of the TP is about twice as strong as that in the eastern TP (Fig. 5(a2)). The AMS is the bias of precipitation and evaporation which represents the precipitation latent heat (formula (5)). By comparing the Fig. 5(a1) and (a2), we can infer that although the AHS is dominated by the precipitation latent heat in the TP, the contribution of AMS to AHS shows large zonal inhomogeneity. The AHS is stronger in the east than in the west, and vice versa for the AMS. This is probably because the surface evapotranspiration is much weaker in the west than in the east (Su [32]), which results in the AMS being smaller in the east than that in the west over the TP. The seasonal variations of the AHS and AMS at high altitude (Fig. 5(b1) and (b2)) are the same as the mean distribution and the value of the AMS and AHS at high altitude are similar because the less is affected by the underlying surface.

The temporal-zonal distribution of the AHS and the AMS in the TIO are basically the same (Fig. 5(c1) and (c2)), which indicates that the AHS is mainly dominated by the precipitation latent heat in this region. In summer, the intensity of the heat sources and moisture sinks are weaker than that in the TP. In addition, the summer atmospheric thermodynamic properties on both sides of 100°E are very different, and the gradient of latitudinal variation is also large. The region of 100°E−120°E, corresponding to Indonesia, is a cold source and moisture source, and the area between 60°E and 100°E is a heat source and moisture sink. The reason for this phenomenon may be related to the distribution of land and sea, and ocean currents.

4.2 *Heat sources spatial distribution and the trend*

The BOB, the southern slope of the TP, and the west of the India Peninsula are the strongest heat sources in summer (Fig. 6(a1)). The strong heat sources in the central and eastern TP in summer is due to latent heating (Fig. 6(a2)). Jiang et al. divided the TP into western, central and eastern domains and reached similar conclusions [12]. For the TIO, there is a strong AHS and AMS in the northwest-southeast direction, which indicates that the AHS is dominated by the precipitation latent heat, and the heat sources and moisture sink centers are located at 10°S near 90°E (Fig. 6(a2)). The heat sources in the TIO, BOB and the TP constitute the meridional distribution, while the AHS in the Arabian Sea, Indian Peninsula, BOB, and Indochina Peninsula constitute the zonal distribution. There are cold source centers located to the southeast of the TIO in summer. Zhang et al. also found that there is an obvious cold source in summer in the southeast of the TIO [20].

In general, the land is a strong AHS in summer, such as the "elevated heat source" of the TP, and the ocean is relatively a weak heat source or a strong heat sink. The intensity of Q_1 in the TP and TIO in July can reach 113 W m^{-2} and 58.4 W m^{-2}, respectively. The

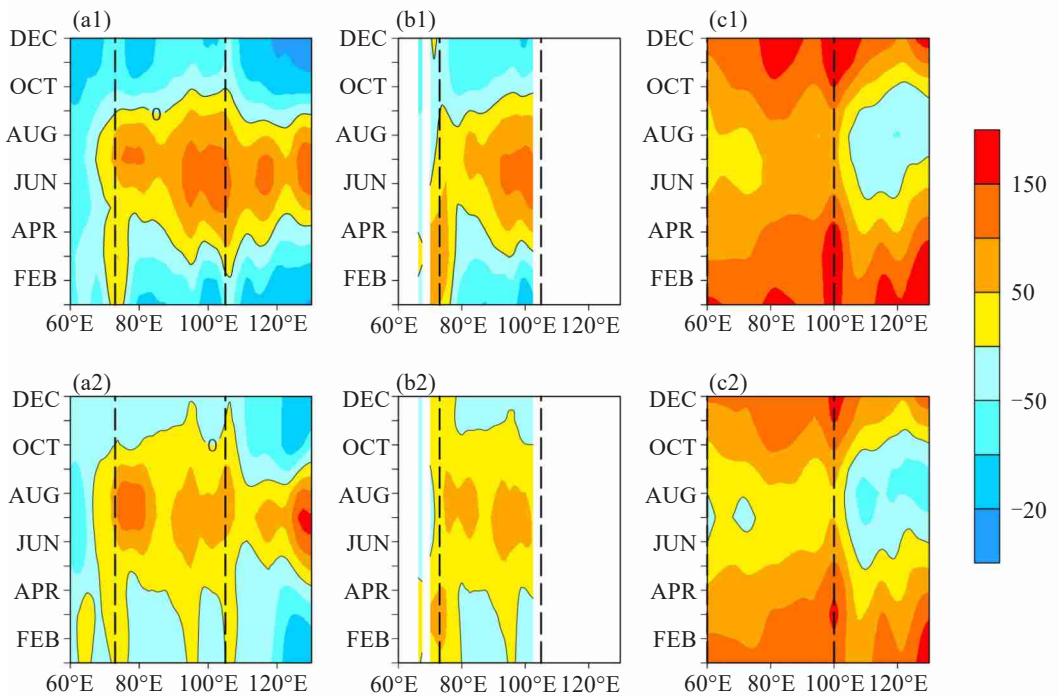

Figure 5. The temporal-zonal distributions of Q_1 (1) and Q_2 (2) from 1980 to 2016 over (a) the TP, (b) the TP altitude ≥2500 m, and (c) the TIO. The black dash lines represent the TP (75°E−103°E) in a1, a2, b1 and b2, and represent the TIO (60°E−100°E) in c1 and c2 (W m^{-2}). The averaged latitudes are 28°N−38°N for the TP and 15°S−5°N for the TIO.

thermal contrast between the sea and land in summer can be measured by the difference in Q_1 between the TP and the TIO. The larger the difference in Q_1, the stronger the meridional thermal contrast.

According to Fig. 6(b1), the TIO Q_1 shows a significant increasing trend (the maximum is about 40 W $m^{-2}10yr^{-1}$), which indicates that the atmospheric heating is significantly enhanced in the area. In the TP, the Q_1 increased on hinterland with the trend about 10 W $m^{-2}10yr^{-1}$, while the southeast of the TP shows a significant decreasing trend (the maximum is about −40 W $m^{-2}10yr^{-1}$). The increasing trend of Q_1 in the TIO is greater than that in the TP, which indicates that the thermal contrast between the TP and the TIO in summer is decreasing. The linear trend distribution of Q_1 has an obvious meridional feature, in that Q_1 at 30°N, 10°−20° N, and 10° S−0° along 90° E has an increasing trend, while Q_2 does not (Fig. 6(b1) and (b2)). The spatial distributions of the linear trends for Q_1 and Q_2 in the TP are different. In addition, both Q_1 and Q_2 are increasing significantly in the BOB.

The Hadley circulation is a fundamental regulator of the earth's energy budget due to the redistribution of energy from tropics to higher latitudes (Liu et al. [33]), and its location and intensity are closely related to the AHS. The TIO Hadley circulation in the southern hemisphere extends across the equator to around 30° N, and the northward mass transport center lies between 0° and 15°S at 600−400 hPa, with an intensity of about −3.5 × 10^9 kg s^{-1} (Fig. 7(a)). The strong ascending branch of the Hadley circulation is located at the south of the TP, while the descend branch lies in 30° S−15° S. The southern hemisphere Hadley circulation shows a weakening trend driven by the strengthened AHS in the TIO (Fig. 6(b1), Fig. 7(b)), while the northern hemisphere Hadley circulation has an increasing trend due to the enhancement of the vertical wind near 15° N (Fig. 7(b)). The decreased winter northern Hadley circulation in the TIO indicates that the meridional energy transported from the tropics in southern hemisphere to the northern hemisphere is reduced.

4.3 *Thermal contrast between the TP and the TIO*

4.3.1 IQ AND $SASM_V$

Due to the decrease of AHS in the southeast and the surrounding of the TP (Fig. 8, Fig. 6 (b1)), the AHS has a weakening trend (Fig. 8). It implies that the ability of the TP heating environment decreases; at the same time, the ascending motion, the lower layer convergence and the upper divergence, and the suction effect of the TP are all weakened (Liu et al. [34]). The southwesterlies over the northern Indian ocean also weakened when the TP heating decreased (Wang et al. [18]).

The TIO AHS shows a significant increasing trend before 1998, and then a weaker decreasing trend (Fig. 8). The IQ (formula (9), where the overbar indicates the regional average) is used to measure the thermal contrast between the TP and the TIO. It shows a significant weakening trend, which indicates that the thermal difference between land and sea decreased quickly. The summer heat source on the TP plays an important role in the formation and evolution of the SASM (Wu et al. [35]). We defined an SASM index ($SASM_V$) by meridional

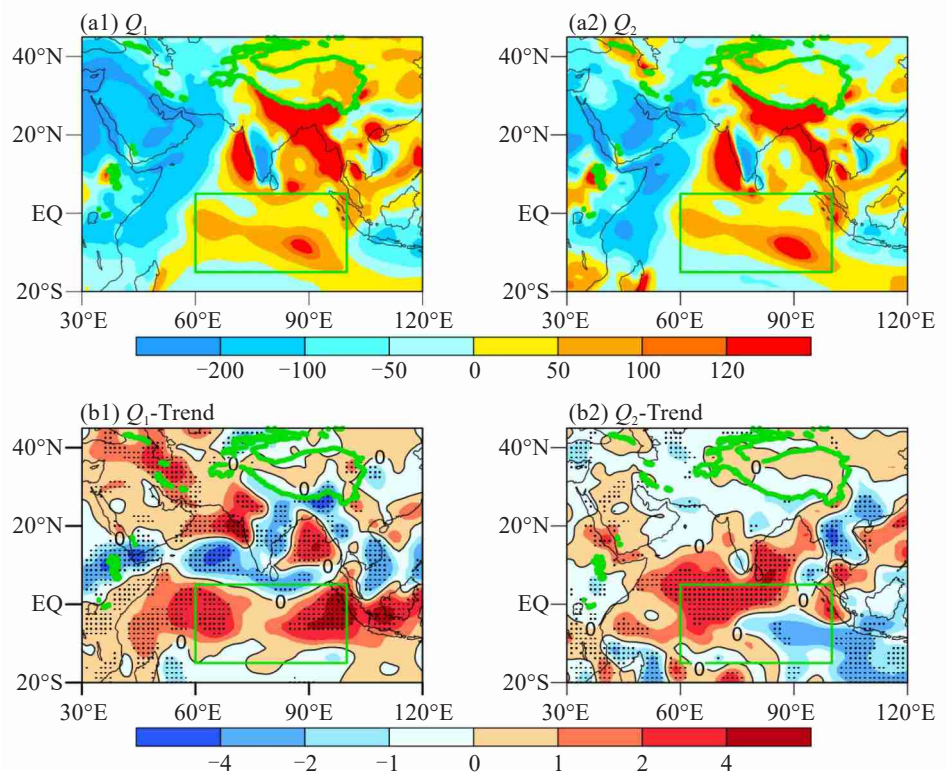

Figure 6. The zonal anomalies of Q_1 (a1) and Q_2 (a2) and their linear trends (b1 and b2, W m^{-2} yr^{-1}) in summer from 1980 to 2016. The TIO is indicated by a green box and the green curve indicates the TP altitude ≥2500 m. The dotted areas passed the 95% significance test.

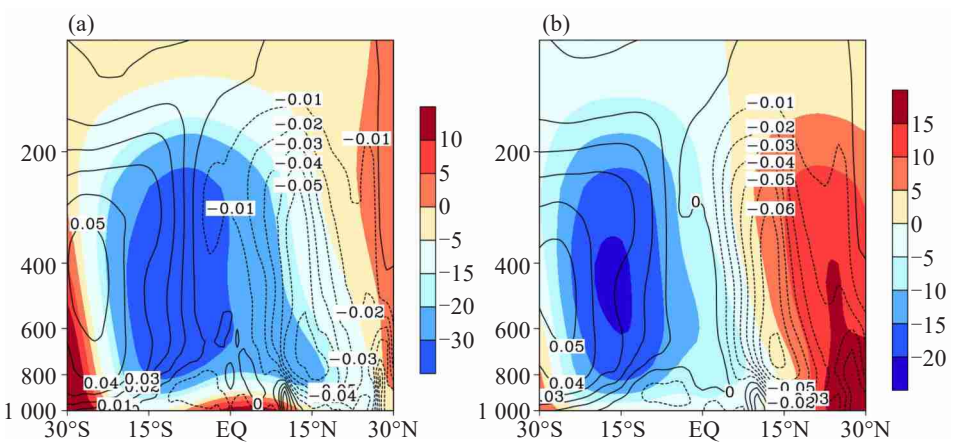

Figure 7. (a) The mass stream function (shaded, units: 10^{10} kg s^{-1}) and vertical velocity (black curve, units: Pa s^{-1}) of zonal averaged along 30°E−100°E in summer from 1980 to 2016. (b) The linear trends (Shaded is mass stream function trend (10^{10} kg s^{-1} yr^{-1}), and black curve is vertical velocity trend (0.01 Pa s^{-1} yr^{-1}).

wind shear between 850Pa and 200hPa (formula (10)). Fig. 8 shows that the SASM-v and the QI are similar in interannual variation. The SASM$_{-v}$ also shows a weakening trend during 1980−2016 and the correlation coefficient between the IQ and SASM$_{-v}$ is 0.801, passing the 95% significance test.

$$IQ = \overline{Q1}_{TP}(75°E-103°E, 28°N-38°N) — \overline{Q1}_{TIO}(60°E-100°E, 15°S-5°N) \quad (9)$$

$$SASM_{-v} = V8_{50hPa} - V_{200hPa}(0°E-20°N, 40°-100°E) \quad (10)$$

4.3.2 INTERANNUAL CHANGE IN THERMAL CONTRAST AND ITS CLIMATE EFFECTS

The TP heating and the Hadley circulation decreased, while the TIO heating increased during 1980−2016, especially during 1980−1998. The IQ shows a significant weakening trend during the period of 1980−1998, whereas during 1999−2016 it maintains a stable low level with no obvious trend (Fig. 8). It indicated that the thermal contrast between the TP and the TIO has changed in the two periods, and during 1999−2016, the

thermal contrasts is weaker. In Fig. 9, the southwest airflow at the lower troposphere and the easterly airflow at the upper troposphere are both weak, which implies that the SASM circulation has weakened during 2007−2016 compared with that during 1980−1989. Hence, as the meridional thermal contrast in the TP-TIO region weakens, the SASM circulation also has weakened.

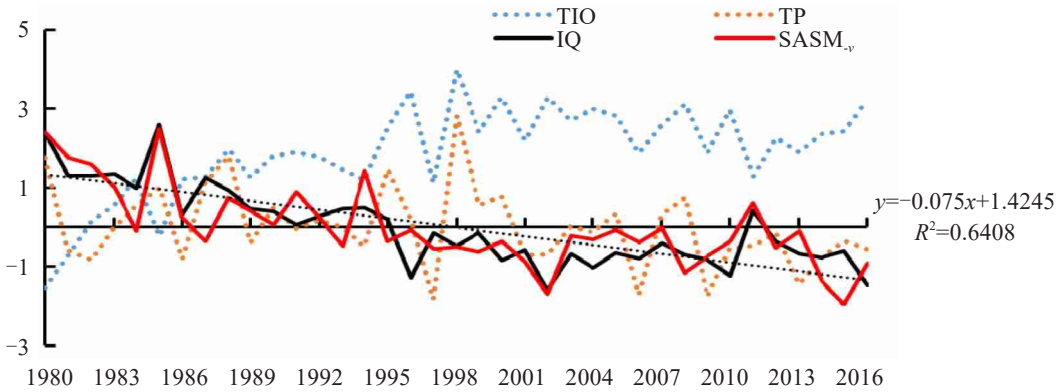

Figure 8. The interannual variations of Q_1 in the TP (The area is in the 75° E−103° E, 28° N−38° N which maskouts the altitude ≥2500m) and the TIO, the IQ, and the $SASM_v$ in summer from 1980 to 2016. The IQ linear trend is shown with a black dotted line and the linear regression coefficient is −0.075. All data are standardized.

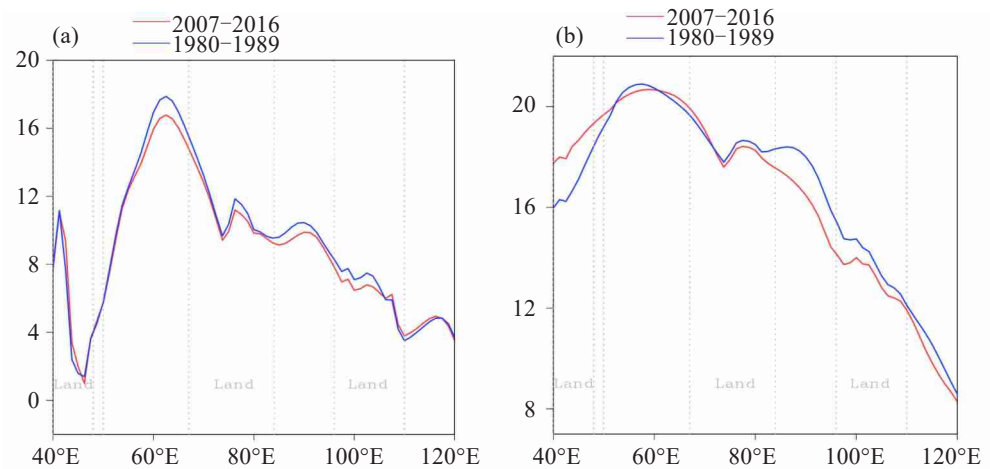

Figure 9. The horizontal wind speed in summer at 15°N ((a):850hPa, (b):200hPa, units: m s^{-1}).

Comparing the period of 2007−2016 with 1980−1989, we find that there is much more precipitation in the Arabian Sea, the BOB, eastern China and the northwest Indian ocean (Fig. 10(a)). The anomaly precipitation with strong convection is in the Arabian Sea and eastern China where an anticyclone and a cyclone appear, respectively (Fig. 10). The two places are the strong water vapor convergence regions (figure omitted). The AHS is an important factor in determining the South Asian High. The position of South Asia High moves westward because the TP AHS decreased and the AHS in the Iran Plateau and the northwest of the Indian Peninsula increased (Fig. 6(b1), Fig. 9(b), Fig. 10(b)). The south slope of the TP, the Indian Peninsula, the central and southern Indochina Peninsula and southeast Indian Ocean have less precipitation associated with anomalous anticyclones.

The equatorial Indian Ocean is controlled by abnormal west wind (Fig. 10(a)), and then the sea temperature rises (figure omitted) though the wind-evaporation-SST feedback (Wang et al. [18]). The increased SST further increases the TIO AHS, resulting in the abnormal ascent flow near 5° S (Fig. 11(a)). Therefore, the TIO southern hemisphere Hadley circulation weakened.

The meridional section of 90° E and the zonal section of 15° N were used to analyze the vertical circulation in the TIO and the BOB (Fig. 11). It can be seen that there is obvious ascending motion in the whole atmosphere in these two places because the AHS increased (Fig. 6(b1)). The enhanced heat sources can trigger two abnormal meridional circulations in the northern 15°S (Fig. 11(a)). The decreased heat source in the south slope of the TP (Fig. 6(b1)) triggers abnormal

downdraft (Fig. 11(a)), resulting in less precipitation. The abnormal zonal circulations appear in the SASM region, with an abnormal descending branch located to the Indian Peninsula and the Indochina Peninsula, and a strong ascending in the BOB (Fig. 11(b)).

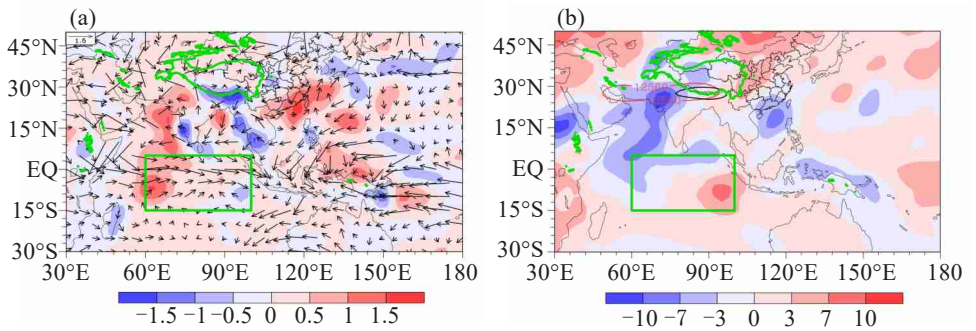

Figure 10. (a) The bias of summer precipitation (shaded, mm d^{-1}) and 850 hPa horizontal wind (vector, m s^{-1}) between 2007−2016 and 1980−1989 in the TP-TIO region. (b) The bias of summer outgoing longwave radiation (shaded, W m^{-2}), and 12560gpm geopotential height (black curve represents 1980−1989, and red curve represents 2007−2016, gpm).

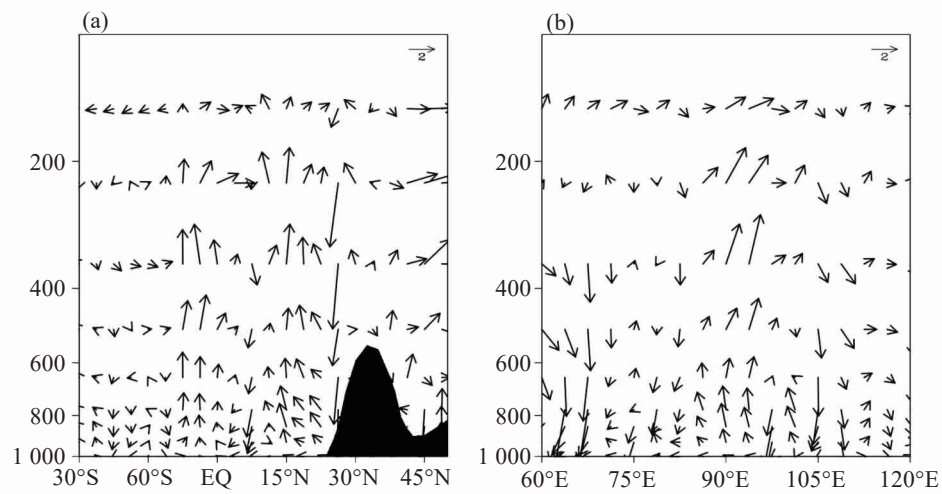

Figure 11. (a) The profile of *v*-*w* wind bias between 2007−2016 and 1980−1989 (along 90°E; units: m s^{-1}). (b) The same as (a), but for *u*-*w* wind (along 15°N; units: m s^{-1}).

5 CONCLUSIONS

The AHS is a comprehensive thermal index of the atmosphere, and its spatial and temporal variations have a significant influence on monsoon circulation. However, quantitative estimation of AHS remains a difficult problem. In this paper, observational data and four sets of reanalysis data were used to calculate the AHS in the TP-TIO region. The statistical correlation analysis shows that the results from the JRA-55 data are closest to the observations. In view of the lack of observations over the TP, the JRA-55 data (1980−2016) were used to study the temporal and spatial distributions of the AHS over the TP-TIO region, and the interannual variation of the land-sea thermal contrast. The major findings are summarized below.

(1) The seasonal variation of the AHS in the TP and the TIO shows great differences. The AHS from April to September is greater than zero in the TP. It reaches the strongest in July and the coldest in January. The TIO is a heat source throughout the year and the monthly variation is "V" shaped. Summer precipitation latent heat is a major contribution to the AHS in the TP-TIO region, and both the AHS and the AMS over the TIO are weaker than those over the TP.

(2) From March to September, there is a heat source center in the east and another one in the west of the TP, and they reach a peak in summer. Both the intensity and extent of the AHS are greater in the east than in the west of the TP, while the AMS shows the opposite pattern. In the TIO, a strong northwest-southeast direction AHS heat center is located near 10° S, 90° E. The thermal properties vary greatly between the east and west sides of 100° E in the TIO region. The linear trend of the summer AHS shows an apparent zonal distribution in the TP-TIO region, while the AMS does not. The AHS increases slightly on the hinterland of the TP, while most of the surrounding areas show a significant decreasing trend.

(3) The IQ is constructed to measure the thermal contrast between the TP and the TIO. It shows a significant decreasing trend, especially before 1998.

Comparing the period of 2007−2016 with 1980-1989, we find the thermal contrast between the TP and TIO is weaker. The equatorial Indian Ocean is controlled by abnormal west wind, and with the wind-evaporation-SST feedback, the increased SST further increases the TIO AHS, resulting in weakened Hadley circulation and SASM circulation. The abnormal meridional circulations appear in the northern TIO and the abnormal zonal circulations in the monsoon region. Finally, there are much more precipitation in the BOB during the weakening thermal contrast period.

This study has discussed the temporal and spatial distributions of the AHS in the TP-TIO region and the interannual variation of the land-sea thermal contrast. Some important conclusions have been drawn, but there are still some problems that require further exploration. There are uncertainties in the indicators of thermal contrast between land and sea (Dai et al. [19]); using height of the troposphere to define the index has an impact on the results. In addition, the average vertical drop between the TP and the TIO is about 4000m, and the maximum heating height in summer is not consistent (figure omitted). Through the thermal wind relationship, it is necessary to further discuss the relationship between the meridional land-sea thermal contrasts and the SASM with its climatic effects.

Acknowledgments: The authors acknowledge the teams for providing the NCEP/DOE, ERA-Interim, MERRA2, JRA-55, and CMA daily data over China, and the GEWEX-SRB data.

REFERENCES

[1] YANAI M, LI C, SONG Z. Seasonal heating of the Tibetan Plateau and its effects on the evolution of the Asian summer monsoon [J]. J Meteorol Soc Japan, 1992, 70(1B): 319-351, https://doi.org/10.2151/jmsj1965.70.1B_319.

[2] YANAI M, TOMITA T. Seasonal and interannual variability of atmospheric heat sources and moisture sinks as determined from NCEP-NCAR reanalysis [J]. J Climate, 1998, 11(3): 463-482, https://doi.org/10.1175/1520-0442(1998)011<0463:SAIVOA>2.0.CO;2.

[3] LI C, YANAI M. The onset and interannual variability of the Asian summer monsoon in relation to land-sea thermal contrast [J]. J Climate, 1996, 9(2): 358-375, https://doi.org/10.1175/1520-0442(1996)009<0358:TOAIVO>2.0.CO;2.

[4] WU G, LIU Y. Thermal adaptation, overshooting, dispersion, and subtropical anticyclone, Part I: thermal adaptation and overshooting [J]. Chin J Atmos Sci, 2000, 24(4): 433-446 (in Chinese).

[5] YAO X, YAN L, ZHANG S. Research progresses and prospects of atmospheric diabatic heating [J]. Meteorol Mon, 2019, 45(1): 1-16 (in Chinese).

[6] YE D, ZHANG J. Preliminary simulation experiment on the influence of heating effect on the East Asian atmospheric circulation over the Tibetan Plateau [J]. Sci China, 1974, 3: 301-320 (in Chinese).

[7] WU G, ZHANG Y. Tibetan Plateau forcing and the timing of the monsoon onset over South Asia and the South China Sea [J]. Mon Wea Rev, 1998, 126(4): 913-927, https://doi.org/10.1175/1520-0493(1998)126<0913:TPFATT>2.0.CO;2.

[8] LUO X, XU J. Estimate of atmospheric heat source over Tibetan Plateau and its uncertainties [J]. Clim Chang Res, 2019, 15 (1): 33-40 (in Chinese).

[9] LUO X Q, XU J J, LI K. A review of atmospheric heat sources over Tibetan Plateau [J]. J Guangdong Ocean University, 2019, 39(6): 130-136 (in Chinese).

[10] XIE J, YU Y, LI J, et al. Comparison of surface sensible and latent heat fluxes over the Tibetan Plateau from reanalysis and observations [J]. Mete Atmos Hys, 2018: 1-18, https://doi.org/10.1007/s00703-018-0595-4.

[11] ZHONG S, WU Z, HE J. Comparisons of the thermal effects of the Tibetan Plateau with NCEP-I and ERA-40 reanalysis data [J]. Atmos-Ocean, 2013, 51(1): 75-87, https://doi.org/10.1080/07055900.2012.755668.

[12] JIANG X, LI Y, YANG S, et al. Interannual variation of summer atmospheric heat source over the Tibetan Plateau and the role of convection around the western maritime continent [J]. J Climate, 2016, 29(1): 121-138, https://doi.org/10.1175/JCLI-D-15-0181.1.

[13] ZHAO P, CHENG L. Climatic characteristics of atmospheric heat source over the Tibetan Plateau in the past 35 years and its relationship with precipitation in China [J]. Sci China (Series D), 2001, 31(4): 327-332, https://doi.org/10.1007/BF02907098.

[14] HU J, DUAN A. Relative contributions of the Tibetan Plateau thermal forcing and the Indian Ocean sea surface temperature basin mode to the interannual variability of the East Asian summer monsoon [J]. Clim Dyn, 2015, 45 (9): 2697-2711, https://doi.org/10.1007/s00382-015-2503-7.

[15] HUANG R, CHEN J, WANG L, et al. Characteristics, processes, and causes of the spatio-temporal variabilities of the East Asian monsoon system [J]. Adv Atmos Sci, 2012, 29(5): 910-942, https://doi.org/10.1007/s00376-012-2015-x.

[16] JI C, ZHANG Y, CHENG Q, et al. On the relationship between the early spring tropical Indian Ocean's sea surface temperature (SST) and the Tibetan Plateau atmospheric heat source in summer [J]. Glob Planet Chang, 2018, 164: 1-10, https://doi. org / 10.1016 / j. gloplacha.2018.02.011.

[17] HE B, LIU Y, WU G, et al. The role of air-sea interactions in regulating the thermal effect of the Tibetan-Iranian Plateau on the Asian summer monsoon [J]. Clim Dyn, 2019, 52(7-8): 4227-4245, https://doi.org/10.1007/s00382-018-4377-y.

[18] WANG Z, DUAN A, YANG S. Potential regulation on the climatic effect of Tibetan Plateau heating by tropical air-sea coupling in regional models [J]. Clim Dyn, 2019, 52: 1685-1694, https://doi.org/10.1007/s00382-018-4218-z.

[19] DAI A G, LI H, SUN Y, et al. The relative roles of upper and lower tropospheric thermal contrasts and tropical influences in driving Asian summer monsoons [J]. J Geophys Res, 2013, 118(13): 7024-7045, https://doi.org/10.1002/jgrd.50565.

[20] ZHANG Y, FAN G, HUA W, et al. Differences in atmospheric heat source between the Tibetan Plateau-South Asia region and the southern tropical Indian Ocean and their impacts on the Indian summer monsoon outbreak [J]. J Mete Res, 2017, 31(3): 540-554, https://

doi.org/10.1007/s13351-017-6042-5.
[21] ZHANG L, XIE Q, YANG X. Interdecadal anomaly of atmospheric diabatic heating and interdecadal weakening of East Asian summer monsoon at the end of 1970s [J]. J Mete Sci, 2015, 35(6): 663-671, https://doi.org/10.1007/s13351-021-0101-7.
[22] DEE D P, UPPALA S M, SIMMONS A J, et al. The ERA-Interim reanalysis: Configuration and performance of the data assimilation system [J]. Quart J Royal Meterol Soc, 2011, 137(656): 553-597, https://doi.org/10.1002/qj.828.
[23] KOBAYASHI S, OTA Y, HARADA Y, et al. The JRA-55 reanalysis: General specifications and basic characteristics [J]. J Mete Soc Japan Ser II, 2015, 93(1): 5-48, https://doi.org/10.2151/jmsj.2015-001.
[24] GELARO R, MCCARTY W, SUÁREZ M J, et al. The modern-era retrospective analysis for research and applications, version 2 (MERRA-2) [J]. J Climate, 2017, 30(14): 5419-5454, https://doi.org/10.1175/JCLI-D-16-0758.1.
[25] KANAMITSU M, EBISUZAKI W, WOOLLEN J, et al. NCEP-DOE AMIP-II Reanalysis (r-2) [J]. Bull Amer Meterol Soc, 2002, 83(11): 1631-1644, https://doi.org/10.1175/BAMS-83-11-1631.
[26] FUJIWARA M, WRIGHT J S, MANNEY G L, et al. Introduction to the SPARC Reanalysis Intercomparison Project (S-RIP) and overview of the reanalysis systems [J]. Atmos Chemi Physi, 2017, 17(2): 1417-1452, https://doi.org/10.5194/acp-17-1417-2017.
[27] HE J H, LI Q, WEI J, et al. Reinvestigations on the East Asian subtropical monsoon and tropical monsoon [J]. Chin J Atmos Sci, 2007, 31: 1257-1265 (in Chinese).
[28] ZHANG B, ZHOU X J, CHEN L X, et al. An East Asian land-sea atmospheric heat source difference index and its relation to general circulation and summer rainfall over China [J]. Science China Earth Sciences, 2010, 53(11): 1734-1746, https://doi.org/10.1007/s11430-010-4024-x.
[29] FENG L, ZHOU T. Water vapor transport for summer precipitation over the Tibetan Plateau: Multidata set analysis [J]. J Geophys Res: Atmos, 2012, 117: D20114, https://doi.org/10.1029/2011JD017012.
[30] DUAN A, SUN R, HE J. Impact of surface sensible heating over the Tibetan Plateau on the western Pacific subtropical high: A land-air-sea interaction perspective [J]. Adv Atmos Sci, 2017, 34(2): 157-168, https://doi.org/10.1007/s00376-016-6008-z.
[31] LIU Y, LI G. Climatic characteristics of atmospheric heat source over the Tibetan Plateau and its possible relationship with the generation of the Tibetan Plateau vortex in summer [J]. Chin J Atmos Sci, 2016, 40(4): 864-876 (in Chinese).
[32] SU T. Research on Spatial-Temporal Variation Characteristics and Its Causes of Global Evaporation Based on Multi-Reanalysis Datasets [D]. Lanzhou: Lanzhou University, 2016 (in Chinese).
[33] LIU J, SONG M, HU Y, et al. Changes in the strength and width of the Hadley Circulation since 1871 [J]. Climate of the Past, 2012, 8(4): 1169-1175, https://doi.org/10.5194/cp-8-1169-2012.
[34] LIU X, LI W, WU G. Interannual variation of the diabatic heating over the Tibetan Plateau and the northern Hemispheric circulation in summer [J]. Acta Meteor Sin, 2002, 16(3): 267-277.
[35] WU G, DUAN A, LIU Y, et al. Tibetan Plateau climate dynamics: recent research progress and outlook [J]. National Science Review, 2014, 2(1): 100-116, https://doi.org/10.1093/nsr/nwu045.

Citation: LUO Xiao-qing, XU Jian-jun, LIU Chun-lei, et al. Characteristics of atmospheric heat sources in the Tibetan Plateau-tropical Indian Ocean region [J]. J Trop Meteor, 2021, 27(1): 70-80, https://doi.org/10.46267/j.1006-8775.2021.007.